Soil moisture and vegetation controls on evapotranspiration in a heterogeneous Mediterranean ecosystem on Sardinia, Italy

Matteo Detto,[1] Nicola Montaldo,[1] John D. Albertson,[2,3] Marco Mancini,[1] and Gaby Katul[2,3]

Received 26 October 2005; revised 19 April 2006; accepted 28 April 2006; published 11 August 2006.

[1] Micrometeorological measurements of evapotranspiration (ET) can be difficult to interpret and use for validating model calculations in the presence of land cover heterogeneity. Land surface fluxes, soil moisture (θ), and surface temperatures (T_s) data were collected by an eddy correlation-based tower located at the Orroli (Sardinia) experimental field (covered by woody vegetation, grass, and bare soil) from April 2003 to July 2004. Two Quickbird high-resolution images (summer 2003 and spring 2004) were acquired for depicting the contrasting land cover components. A procedure is presented for estimating ET in heterogeneous ecosystems as the residual term of the energy balance using T_s observations, a two-dimensional footprint model, and the Quickbird images. Two variations on the procedure are successfully implemented: a proposed two-source random model (2SR), which treats the heat sources of each land cover component separately but computes the bulk heat transfer coefficient as spatially homogeneous, and a common two-source tile model. For 2SR, new relationships between the interfacial transfer coefficient and the roughness Reynolds number are estimated for the two bare soil–woody vegetation and grass–woody vegetation composite surfaces. The ET versus θ relationships for each land cover component were also estimated, showing that that the woody vegetation has a strong tolerance to long droughts, transpiring at rates close to potential for even the driest conditions. Instead, the grass is much less tolerant to θ deficits, and the switch from grass to bare soil following the rainy season had a significant impact on ET.

Citation: Detto, M., N. Montaldo, J. D. Albertson, M. Mancini, and G. Katul (2006), Soil moisture and vegetation controls on evapotranspiration in a heterogeneous Mediterranean ecosystem on Sardinia, Italy, *Water Resour. Res.*, *42*, W08419, doi:10.1029/2005WR004693.

1. Introduction

[2] Semiarid regions, such as around the Mediterranean, suffer from broad desertification processes produced by both natural (climate variations, fires, etc.) and human (deforestation, overgrazing, urbanization, pollution, fires, etc.) influences [*Brunetti et al.*, 2002; *Lelieveld et al.*, 2002; *Moonen et al.*, 2002; *Mouillot et al.*, 2002; *Ventura et al.*, 2002; *Ceballos et al.*, 2004].

[3] In these regions, the root zone soil moisture is a key control on the surface water and energy balances [*Entekhabi et al.*, 1996; *Western et al.*, 2002; *Albertson and Montaldo*, 2003], and thus further controls the recharge of groundwater and surface water that may serve as drinking water reservoirs [*Sophocleous*, 2000; *Ragab et al.*, 2001]. In semiarid regions evapotranspiration (ET) is the leading loss term of the root zone water budget with a yearly magnitude that may be roughly equal to the precipitation [*Reynolds et al.*, 2000; *Rodriguez-Iturbe*, 2000; *Baldocchi et al.*, 2004; *Kurc and Small*, 2004; *Maselli et al.*, 2004; *Williams and Albertson*, 2004].

[4] These Mediterranean ecosystems are commonly heterogeneous savanna-like ecosystems, with contrasting plant functional types (PFTs, e.g., grass, shrubs and trees) competing for the water use [*Scholes and Archer*, 1997; *Ramirez-Sanz et al.*, 2000; *Jackson et al.*, 2002; *Baldocchi et al.*, 2004; *Fernandez et al.*, 2004; *Williams and Albertson*, 2004]. Despite the attention these ecosystems are receiving, a general lack of knowledge persists about the relationship between ET and the plant survival strategies for the different PFTs under water stress [*Baldocchi et al.*, 2004; *Kurc and Small*, 2004]. With this as motivation, we explore the issue of estimating ET and its relationship with soil moisture, θ, for the typical PFTs of an heterogeneous water-limited Mediterranean ecosystem. This is an important ecohydrological issue [*Rodriguez-Iturbe*, 2000; *Albertson and Kiely*, 2001; *Williams and Albertson*, 2004; *Montaldo et al.*, 2005] for both prognostic models, in which predictions of θ and land surface fluxes (e.g., ET) are required for a projected radiative and precipitation forcing time series, and diagnostic models, in which land surface fluxes are

[1] Dipartimento di Ingegneria Idraulica, Ambientale, Infrastrutture viarie e del Rilevamento, Politecnico di Milano, Milan, Italy.
[2] Department of Civil and Environmental Engineering, Pratt School of Engineering, Duke University, Durham, North Carolina, USA.
[3] Nicholas School of the Environment and Earth Sciences, Duke University, Durham, North Carolina, USA.

0043-1397/06/2005WR004693$09.00

estimated for a set of observed atmospheric and surface states (θ and surface temperature, T_s) using satellite remote sensing observations [*Montaldo et al.*, 2001; *Kustas et al.*, 2002; *Caparrini et al.*, 2004; *Reichle et al.*, 2004]. Regarding the diagnostic perspective, the mapping of surface θ at high spatial resolutions may be derived from active microwave sensor (radar) observations (up to 10 m of spatial resolution); however the uncertainties on the effectiveness of the radar signal remain large, especially in heterogeneous terrain [e.g., *Altese et al.*, 1996; *Mancini et al.*, 1999; *Holah et al.*, 2005]. While more accurate θ estimates may be provided by passive microwave remote sensor observations, they are at extremely coarse spatial resolutions (25–50 km) [*Jackson*, 1997a; *Entekhabi et al.*, 2004], arguably unsuited to heterogeneous Mediterranean ecosystems. Instead, estimates of T_s from passive remote sensors (at infrared bands) are more attractive because they are more robust and also available at higher spatial resolutions: for instance, images from the AVHRR sensor are at 1100 m spatial resolution and daily temporal resolution, while images of the ASTER sensor mounted on Terra satellite are at 90 m spatial resolution and 16-day temporal resolution [*Dash et al.*, 2002; *Kustas et al.*, 2003]. For this reason, we investigate the possibility to estimate land surface fluxes from T_s remote observations in heterogeneous ecosystems.

[5] Given that shifts in vegetation cover vary with hydrologic controls, observation of water and energy fluxes must be conducted through extended field campaigns [e.g., *Jackson*, 1997b; *Halldin et al.*, 1999; *Albertson and Kiely*, 2001; *Montaldo et al.*, 2003; *Kurc and Small*, 2004]. Recent efforts [*Baldocchi et al.*, 2004; *Kurc and Small*, 2004; *Williams and Albertson*, 2004] compared spatially aggregate ET estimates in grasslands and shrublands from micrometerological observations [e.g., *Brutsaert*, 1982; *Garratt*, 1992], and estimated the relationships between ET and θ for the two contrasting ecosystems. However, in heterogeneous ecosystems with various land cover components, micrometeorological observations need to be carefully interpreted. Indeed, since the tower flux measurements are often conducted at a height comparable to the patchiness length scale, thus putting the characteristic transporting eddy on a similar length scale as the surface heterogeneity, the measured fluxes are not so trivially interpreted in terms of the contributing source areas (or PFTs).

[6] The most elementary approach, as taken in most of the references cited above, is to assume the observed ET rates from the tower are representative of the large-scale average land cover characteristics (i.e., the ecosystem), with a single temporally constant value for the fractional cover of each PFT. This simplification misses several important aspects: (1) the source area of each land cover component contributing to the flux measurement may vary during the observation period; (2) the separate and unique forms of ET = ET (θ) for each PFT remain undefined, (3) the results are not transferable to other sites with different percentage of cover of PFTs. These are important issues because due to human and natural influences the distributions of PFTs vary spatially and temporally over the Mediterranean regions [*Scholes and Archer*, 1997; *Fernandez et al.*, 2004].

[7] The combination of recent advancements in footprint models [*Schmid*, 1994; *Hsieh et al.*, 2000; *Schmid*, 2002; *Finnigan*, 2004; *Kljun et al.*, 2004] and high-resolution remote sensing of the land surface presents a promising path toward interpreting land surface flux estimates from models with tower-based micrometeorological observations in heterogeneous ecosystems. The concept of a footprint became popular in the last decade because it provides a quantitative interpretation of the field of view of tower-based eddy correlation instruments. At the same time new satellite remote sensors are permitting unprecedented spatial resolution (up to 1 m) mapping of land cover from visible (VIS) and near infrared (NIR) bands [*Su et al.*, 2004], and ground-based thermal infrared thermometers permit the monitoring of skin temperature for the constitutive elements (e.g., PFTs) of the land surface [e.g., *Williams and Albertson*, 2004]. These thermal sensors provide analogous information to those of satellite thermal infrared sensors (simply placed meters from a source rather than tens or hundreds of kilometers).

[8] We propose to use micrometeorological measurements, ground based thermal infrared thermometers, and high-resolution VIS/NIR remote observations to estimate land surface fluxes of each cover type, and then to use an adapted 2-D version of the analytical footprint model of *Hsieh et al.* [2000] (hereafter indicated with H2000) to aggregate the fluxes appropriately for comparison to the tower measured fluxes. The model-derived surface fluxes are used with the observed soil moisture data to estimate the relationships between θ and ET for each constitutive PFT on the landscape.

[9] A logical starting point is a patchy landscape dominated by only two elements: bare soil and woody vegetation or grass and woody vegetation. Despite its simplicity such dual-PFT landscapes are fairly common in water-limited ecosystems. The case study site is within the Flumendosa basin on Sardinia, which is one of the regions of Italy most affected by water deficits, and indeed the recent long-term drought on the island has raised serious concerns about climate change and land use impacts on the water resources of the region. There is therefore an urgent need to exploit advanced observation and simulation technologies to provide a better understanding of the water balance regime for the entire island and for its major catchments. In this sense, the Flumendosa river basin constitutes the water supply for much of southern Sardinia, including the island's largest city, Cagliari (about 350,000 inhabitants in the urban area).

[10] In this way, the following objectives are addressed: (1) assess the usefulness of surface temperature measurements in concert with revised interfacial transfer theories for heterogeneous landscapes for estimating evapotranspiration over heterogeneous water-limited terrains and (2) identify the functional relationship between soil water content and evapotranspiration for the individual landscape components (i.e., woody vegetation, grass and bare soil).

2. Experiment

[11] The site, the tower setup and instruments, and the remote sensing images are described next.

2.1. Site

[12] The measurements were conducted at a site in Orroli (39° 41′ 12. 57″ N, 9° 16′ 30. 34″ E, 500 m a. s. l.), situated in the mideast of Sardinia (Italy). The site (area $\sim$ 1.5 km^2) is a plateau that has a gentle slope (approximately 3°) from

NW to SE. The landscape is a patchy mixture of Mediterranean vegetation types: trees, including mainly wild olive (*Olea sylvestris*) of height approximately 3.5–4.5 m, and several cork oaks (*Quercus suber*) of height approximately 6–7 m, several different types of shrubs (e.g., *Asparagus acutifolius, Rubus ulmifolius*) and herbaceous (grass) species (e.g., *Asphodelus microcarpus, Ferula comunis, Bellium bellidioides, Scolymus hispanicum*) that are present in live form only during wet seasons and reach heights of approximately 0.5 m. The soil thickness varies from 15–40 cm, bounded from below by a rocky layer of basalt. This impervious layer leads to tree and shrub rooting systems that expand horizontally. The soil is mainly silt loam with a bulk density of 1.38 g/cm^3 and a porosity of 53%. The root zone depth is coincident with the soil depth for these thin soils. The foliage density of the woody vegetation (trees and shrubs) remains approximately constant throughout the year (woody leaf area index, LAI, fluctuates between 3.5 and 4.5), whereas, the leaf area of the herbaceous species increases rapidly with winter and spring precipitation (maximum grass LAI of 2) and vanishes for the summer.

[13] The climate at this site is typically Mediterranean maritime, with a mean historical (1922–1992) annual precipitation of 690 mm (rain gauge data from the nearby village of Nurri), and mean historical monthly precipitations ranging between 103 mm in December and 12 mm in July. Furthermore, historical air temperature data of the Nurri station are mean annual value of 13.9°C, mean monthly values ranging between 23.1°C in July and 6.1°C in January.

2.2. Tower Setup

[14] A 10 m tower was instrumented to measure land-atmosphere fluxes of energy, water, and carbon in addition to key state variables. The tower was anchored to a small outcropped rock, surrounded by wild olive trees, grass and bare soils (depending on the year season). Data are available from April 2003 to July 2004.

[15] A Campbell Scientific CSAT-3 sonic anemometer and a Licor-7500 CO_2/H_2O infrared gas analyzer were used to measure velocity and gas concentrations at 10 Hz for the estimation of latent heat (LE), and sensible heat fluxes (H) through standard eddy correlation methods [e.g., *Brutsaert*, 1982; *Garratt*, 1992]. The two instruments were placed at 10 m height above the ground. Half hourly statistics were computed and recorded by a 23X data logger (Campbell Scientific Inc., Logan, Utah). The effect of the gentle slope of the plateau was removed by an axis rotation (equations are presented in Appendix A for completeness) analogous to an approach used in other studies on complex topography [*Baldocchi et al.*, 2000]. The Webb-Pearman-Leuning adjustment [*Webb et al.*, 1980] was later applied.

[16] Three infrared transducers, IRTS-P (Apogee Instrument, accuracy of 0.3°C) were used to measure the surface temperature (T_s) of the different PFTs. One IRTS-P observed the skin temperature of a tree (wild olive) canopy at 3.5 m height above the ground and with a canopy view zenith angle of about 70°, another observed either bare soil or grass (depending on the season) at 1.6 m above the ground with a canopy view zenith angle of about 50°, and the third sensor was placed at a greater height (10 m above the ground, view zenith angle of about 40°) to observe a composite mixture of trees and soil or trees and grasses

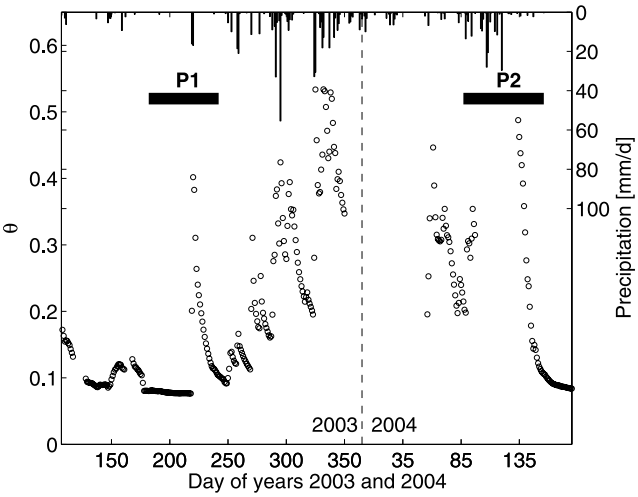

Figure 1. Mean daily root zone soil moisture (open circle) and precipitation (bar) recorded at the Orroli tower. The two investigated periods, P1 and P2, are also highlighted.

(depending on the year season). In these transducers T_s is derived from the apparent target temperature through calibration relationships, which depend on the sensor body temperature [*Bugbee et al.*, 1998], and are provided by the manufacturer.

[17] The incoming and outgoing shortwave and longwave radiation components were measured by a CNR-1 (Kipp & Zonen) integral radiometer positioned at 10 m with a hemispherical field of view. Soil heat flux (G) was measured at two different locations close to the tower, one in an open patch (4 m from the tower) and one under a tree canopy of wild olive (5.5 m from the tower), with thermopile plates, HFT3 (REBS), buried at 8 cm below the soil surface. Two thermocouples (per plate) were buried at 2 and 6 cm, and one frequency domain reflectometer probe (FDR Campbell CS615) per plate was buried horizontally at 5 cm, as needed to estimate changes in the stored energy above the plates (see HFT3 instruction manual edited by Campbell Sci.).

[18] A total of seven FDR probes were buried close to the tower (3.3–5.5 m away) to estimate the mean θ within the root zone. Four were buried horizontally (two at 15 cm depth and two at 5 cm) and three were installed vertically (i.e., average 0–30 cm).The FDR calibration ($\theta = 2.755 - 7.875\,\tau + 7.259\,\tau^2 - 2.002\,\tau^3$, with τ the FDR probe output period in milliseconds) was made using gravimetric water content sampled (a total of 11 samples during the entire period of observation) near the probes over a wide range of soil moisture conditions ($0.08 < \theta < 0.55$).

[19] Precipitation was measured by an ARG100 (Environmental Measurements Limited) rain gauge. Recorded precipitation and θ time series (aggregated to the daily scale) are shown in Figure 1. Data gaps (22.7% of the total half hour values) exist mainly due to power supply failures and maintenance operations. Rainfall observations during the data gaps are filled with rainfall data of a nearby rain gauge located in the town of Nurri.

2.3. Remote Sensing Images

[20] Two multispectral high spatial resolution (2.8 m × 2.8 m per pixel) Quickbird satellite images (DigitalGlobe

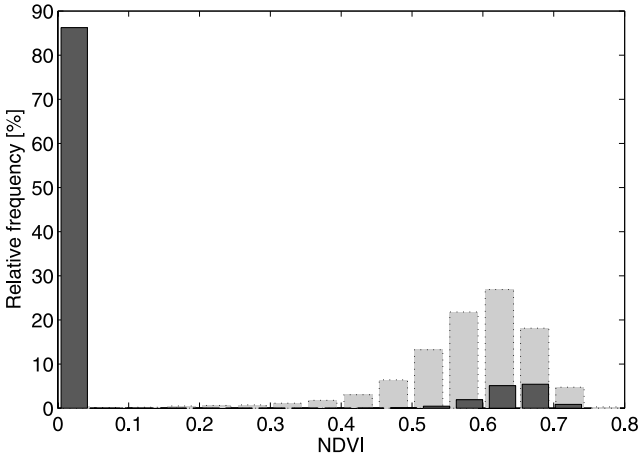

Figure 2. Distributions of the NDVI relative frequencies of the two Quickbird satellite images at DOY = 220, 2003 (solid bar) and DOY = 138, 2004 (gray bar with dotted line).

Inc.) were acquired (DOY = 220, 2003 and DOY = 138, 2004). The two images depict the contrasting land covers of the summer and the spring, respectively, which are key seasons in the water resources management of Mediterranean ecosystems. Indeed, the first image characterizes the land cover after a long dry period just before a significant rain event (Figure 1), so that the soil moisture conditions were very dry ($\theta \approx 0.08$) and herbaceous cover was absent such as is typical in the Sardinian summer. The second image depicts the land cover conditions after a long wet period ($\theta \approx 0.4$, Figure 1), hence the bare soil was nearly absent because of the flourishing grasses that in those days reached their maximum growth.

[21] The 6S model of *Vermote et al.* [1997] was used to correct the images for atmospheric effects. The input parameters for the 6S model were: midlatitude atmosphere model, maritime aerosol model, horizontal visibility of 40 km, and inhomogeneous ground surface reflectance. A supervised classification scheme based on the parallepiped algorithm [*Richards*, 1999] allows for distinguishing "woody vegetation" (WV) from "nonwoody vegetation" (NWV, i.e., bare soil or grass according to the time period) from the image of DOY = 220, 2003. The widely used normalized difference vegetation index (NDVI) [e.g., *Gamon et al.*, 1995; *Carlson and Ripley*, 1997; *Scanlon et al.*, 2002] was computed from the surface reflectance values averaged over ranges of wavelengths in the visible red and NIR regions of the spectrum. Figure 2 shows the comparison of the distributions of the NDVI relative frequencies of the two images in the field around the tower (area of 1300 m $\times$ 1300 m), highlighting the contrast between the land covers of the two periods. While on DOY = 220 of 2003 bare soil (i.e., NDVI equal 0) was the dominant cover type (almost 90%), it was absent on DOY = 138 of 2004.

[22] The $NDVI/NDVI_{MAX}$ map (where $NDVI_{MAX}$ is the spatial maximum of the particular NDVI map) of the field around the tower (the tower is in the center of the map) for the DOY = 220, 2003 is computed (Figure 3a). Note that $NDVI/NDVI_{MAX}$ values of WV pixels are greater than 0.6, so that the color bar of the Figure 3a is modified for a better contrast of the WV pixels. The heterogeneity of the field is well depicted by Figure 3b, which shows the spatial average of $NDVI/NDVI_{MAX}$ within circles of variable radius (for increments of 14 m) centered at the tower. It is clear from Figure 3 that the tower resides in a preferentially dense vegetation area, with the values of $\frac{NDVI}{NDVI_{MAX}}$ decreasing from about 0.4 (close to the tower) to 0.1. Beyond the radial bias, we also note a directional effect of heterogeneity in Figure 3a.

[23] Hereafter we focus on two periods, P1 and P2 as noted in Figure 1, bounding the image acquisition dates, because the two periods allow for an evaluation of the land surface fluxes in two contrasting ecosystem conditions: the first period is in the summer (DOY = 187–242, 2003), with the surface dominated by bare soil and WV (P1); the second period is in the spring (DOY = 87–156, 2004) with the surface primarily dominated by grass and WV (P2). Hence, in each analysis period we consider a patchy landscape with only two elements (WV and NWV), with NWV being bare soil during P1 and grass during P2. This simplified approach is a necessary first step toward building a comprehensive approach for multielement ecosystems on complex terrain. Note that in P2 there is a significant data gap (DOY = 98–133, 2004), unfortunately.

[24] Figure 4 reports the hourly average values of air and surface temperatures during the daytime of the two selected periods highlighting the significant difference in temperature conditions between the two periods and among the ecosystem land cover components. As expected, the data show that during P1 the difference between the T_s of bare soil and the T_s of WV is significantly larger than the difference between the T_s of grass and the T_s of WV during P2. This is an important consideration for spatially downscaling satellite data of radiometric surface temperatures in these landscapes.

39

3. Theoretical Development

[25] For the stated objectives, estimates of the energy flux contribution of each landscape component are necessary. While it is true that the footprint (source area) of eddy correlation flux measurements changes in size and directionality through time, this variation can be exploited to sample the relative fractions of the different surface types.

[26] Hence the first step is to introduce the concept of footprint for establishing an objective connection between individual PFT-based surface flux model calculations and the measured aggregate fluxes by the eddy correlation system. The combined use of a footprint model and the high-resolution satellite image allows us to distinguish the source area of each PFT to the measured flux. Then, the methodology for 1) estimating energy fluxes from T_s (and meteorological) observations over heterogeneous terrains, and 2) evaluating hydrologic relationships between θ and derived ET estimates for each landscape component are described.

3.1. Footprint Model for Interpreting Surface Flux Observations

[27] In a coordinate system (x, y, z) referenced at the tower base, a source distribution S_Φ at the ground is related

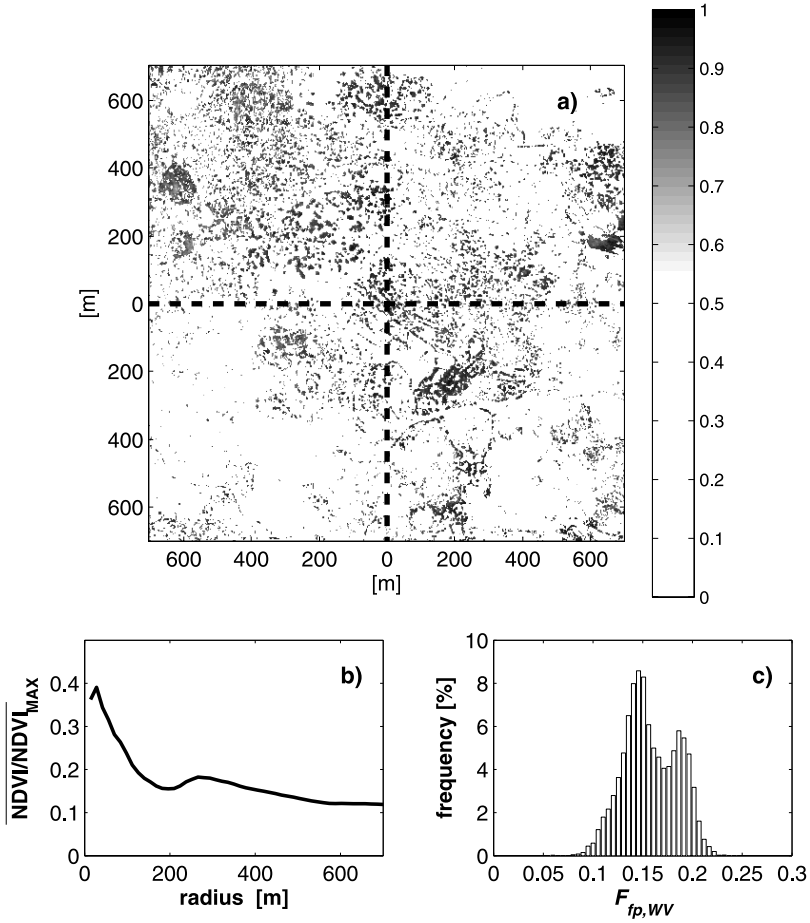

Figure 3. (a) Map of NDVI/$NDVI_{MAX}$ of WV of the field around the tower (the tower is in the center of the map) determined from the Quickbird image (spatial resolution 2.8 m × 2.8 m) for DOY = 220, 2003; note that NDVI/$NDVI_{MAX}$ values of WV pixels are greater than 0.6, so that the color bar is modified for a better contrast of the WV pixels. (b) NDVI/$NDVI_{MAX}$ average values of the fields within a circle around the tower versus radial distance from the tower. (c) Histogram of the time series of $F_{fp,WV}$ of the whole data set.

to the observed surface flux Φ_{obs} (e.g., H, LE, or the radiation) by [*Schmid*, 1997]:

$$\Phi_{obs}(0,0,z_m) = \int_0^{\infty}\int_0^{\infty} S_{\Phi}(x,y,0) f(x,y,z_m) dxdy \qquad (1)$$

where z_m is the height of measurement, $f(x, y, z_m)$ is the source area function, which, for instance, depends on the features of the turbulent flow (e.g., roughness properties, stability of the air and wind direction) in the case of micrometeorological observations and on the properties of the instrument in the case of the radiometer [*Schmid*, 1997].

[28] If the landscape is decomposed into its constitutive elements, we can discretize the integral equation (1) on a uniform grid of $M \times N$ dimensions (note that Φ_{obs} and f depend on z_m, but hereafter we avoid to repeat this notation):

$$\Phi_{obs} \cong \sum_{k=1}^{n_e} S_{\Phi,k} \sum_{i=1}^{N}\sum_{j=1}^{M} f_{ij}\xi_{ijk}\Delta x\Delta y \qquad (2)$$

where n_e is the number of the constitutive elements (in our case $n_e = 2$ since we have NWV and WV), ξ_{ijk} is the fraction of the kth cover type in the i-j grid cell, Δx and Δy are the pixel dimensions, $S_{\Phi,k}$ is the source strength for the kth cover type, and f_{ij} is the value of the source area function for the i-j grid cell.

[29] Rearranging equation (2) we obtain

$$\Phi_{obs} \cong \sum_{k=1}^{n_e} S_{\Phi,k} F_{fp,k} \qquad (3)$$

where the $F_{fp,k}$ is the fraction of the kth cover type in the footprint

$$F_{fp,k} = \sum_{i=1}^{N}\sum_{j=1}^{M} f_{ij}\xi_{ijk}\Delta x\Delta y \qquad (4)$$

[30] In the case of eddy correlation measurements Φ_{obs} is, for instance, the observed H, LE. Several models have already been proposed for f [*Schmid*, 2002; *Vesala et al.*, 2004]. We adopt the H2000 simplified analytical model modified to include lateral dispersion. The proposed model

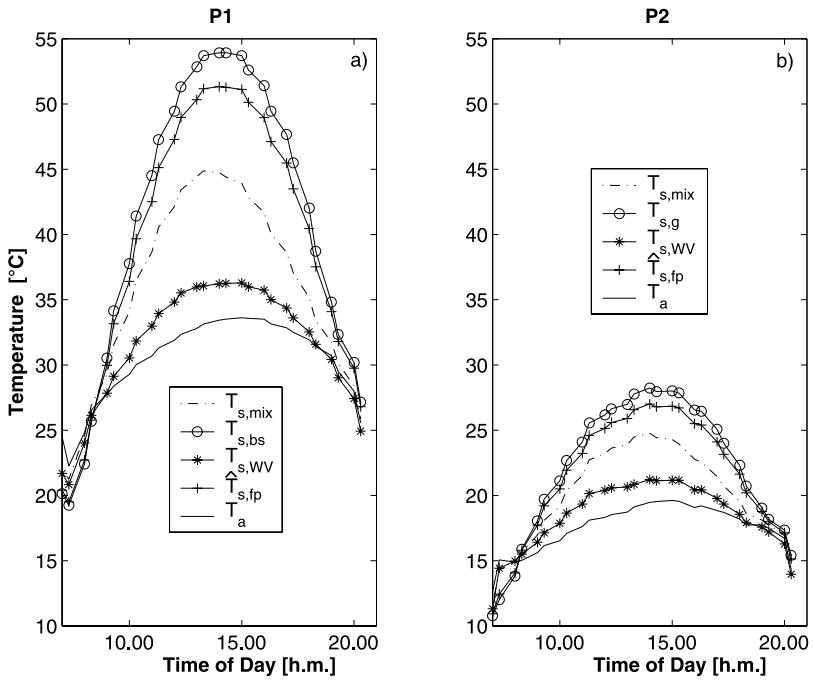

Figure 4. Diurnal variation of the ensemble-averaged ground-based IRT temperatures during the two periods for individual WV ($T_{s,WV}$), bare soil ($T_{s,bs}$), grass ($T_{s,g}$) and the composite surface temperature (referred to as $T_{s,mix}$), and the footprint weighted surface temperature value ($\hat{T}_{s,fp}$). For reference the observed air temperature (T_a) at z_m = 10 m is also shown (solid line).

has been tested against several data sets [e.g., *Baldocchi and Rao*, 1995]. Appendix B describes how lateral dispersion was included in the H2000 model. For illustration, we present the cross-wind integrated footprint (F^y) and the contour line of the 50% flux source area (i.e., 50% of the measured flux comes from within this boundary) to demonstrate the extent of longitudinal and lateral spread for mildly stable (Obukhov's length, L, of 100 m, friction velocity, u_*, of 0.5 m/s and standard deviation of the velocity component along the vertical axis, σ_v, of 0.6 m/s) and mildly unstable (L = −100 m, u_* = 0.5 m/s and σ_v = 0.6 m/s) atmospheric stability conditions (Figure 5).

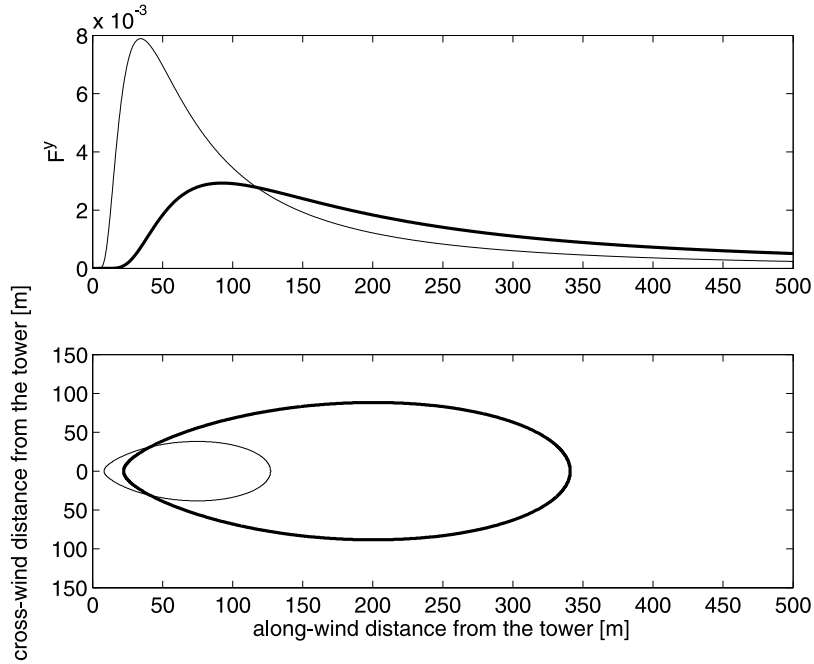

Figure 5. (top) Cross-wind-integrated footprints (F^y) for mildly unstable (thin line) and mildly stable (thick line) conditions. (bottom) Contour lines representing the 50% flux source area for the two footprints of Figure 5 (top).

[31] Instead, in the case of the radiative flux observations (i.e., for the radiometer), f is given by the optical source weight function of the instrument [*Schmid*, 1997]:

$$f = \frac{1}{\pi}\left(z_m + \frac{r_d^2}{z_m}\right)^{-2} \tag{5}$$

where r_d is the radial distance from the radiometer center. In this case $F_{fp,k}$ is constant through time.

3.2. Estimation of the Energy Balance Fluxes

[32] Here we present a forward model that will estimate fluxes for each PFT and aggregate them to the tower footprint for subsequent comparison to measured fluxes (which are of course footprint specific). Surface fluxes "at the tower", for any particular time period, are predicted through

$$\hat{\Phi} = \sum_{k=1}^{n_e} \hat{S}_{\Phi,k} F_{fp,k} \tag{6}$$

where $\hat{\Phi}$ is the estimated surface flux, $F_{fp,k}$ is given by (4), and $\hat{S}_{\Phi,k}$ is the estimated flux contribution of the kth cover type (described below).

[33] For calculating $F_{fp,k}$ we need to estimate ξ_{ijk} in (4), with $n_e = 2$ in our case. Note that the value ξ_{ijk} for WV land cover ($\xi_{ij,WV}$) may be less than 1 according to the WV density in the pixel (see section 2.3). Because NDVI and the fraction of vegetation cover are strongly related [e.g., *Gutman and Ignatov*, 1997; *Shimabukuro et al.*, 1997] we adopt $\xi_{ij,WV} = \mathrm{NDVI}_{ij}/\mathrm{NDVI}_{\mathrm{MAX}}$, where NDVI_{ij} is the NDVI value of the generic grid cell (Figure 3a) and, i.e., $\xi_{ij,NWV} = 1 - \xi_{ij,WV}$ for NWV cover.

[34] We now present the methodology for estimating $\hat{S}_{\Phi,k}$ of each energy balance term.

3.2.1. Available Energy

[35] The available energy of the kth cover type is $\hat{S}_{Qn,k} = \hat{S}_{Rn,k} - \hat{S}_{G,k}$, with $\hat{S}_{Rn,k}$ and $\hat{S}_{G,k}$ the estimated R_n and G contributions of the kth cover type, respectively. $\hat{S}_{Rn,k}$ is estimated from the measurements of the incoming shortwave ($R_{sw,in}$) and longwave radiation ($R_{lw,in}$) fluxes and the T_s of the kth cover type ($T_{s,k}$) as [e.g., *Brutsaert*, 1982]

$$\hat{S}_{Rn,k} = R_{sw,in}(1 - \alpha_k) + \varepsilon_k\left(R_{lw,in} - \sigma T_{s,k}^4\right) \tag{7}$$

where α_k and ε_k are the surface albedo and emissivity of the kth cover type, respectively, and σ is the Stefan-Boltzmann constant. When reflected shortwave and emitted longwave radiation observations and surface temperature observations are available α_k and ε_k may be accurately estimated through calibration.

[36] $\hat{S}_{G,k}$ is estimated as a fraction of $\hat{S}_{Rn,k}$, given by

$$\hat{S}_{G,k} = c_k \hat{S}_{Rn,k} \tag{8}$$

where we assume constant values of c_k for the different land cover types, which is an acceptable assumption at daily timescale [e.g., *Brutsaert*, 1982]. Also c_k may be accurately estimated through calibration using soil heat flux observations.

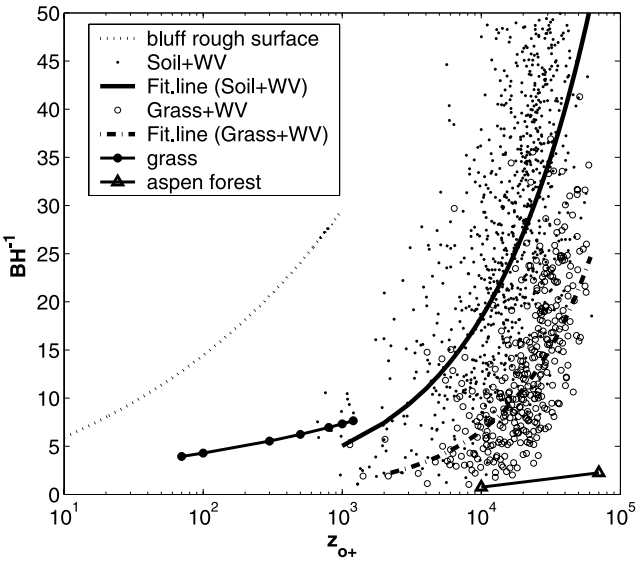

Figure 6. B_H^{-1} values estimated from observed data using (12) versus z_{o+} for the composite soil-WV and grass-WV surfaces. For reference, published B_H^{-1} values for bluff rough surface, grass, and an aspen forest are reported.

3.2.2. Sensible Heat Flux

[37] The estimated sensible heat flux contribution of the kth cover type ($\hat{S}_{H,k}$) is computed from the bulk transfer formulation [*Garratt*, 1992]:

$$\hat{S}_{H,k} = C_{hr}\rho c_p u\left(T_{s,k} - T_a\right) \tag{9}$$

where ρ is the temporal mean air density, c_p is the specific heat capacity of dry air at constant pressure, u and T_a are the wind speed and air temperature, respectively, and C_{hr} is the transfer coefficient that relates directly the sensible heat flux and the radiative surface temperature of each land cover type in our analysis. Note that in the bulk transfer formulation $\hat{S}_{H,k}$ is not related to T_s but to the aerodynamic surface temperature of the Monin-Obukhov similarity theory [e.g., *Brutsaert*, 1982]. C_{hr} is related to the interfacial transfer coefficient, often referred to as $k_v B_H^{-1}$ [*Brutsaert*, 1982; *Garratt*, 1992] with k_v (=0.4) the von Karman's constant, through

$$C_{hr} = \frac{Cd_m^{0.5}}{B_H^{-1} + Cd_m^{-0.5}} \tag{10}$$

where Cd_m $(=u_*/u)^2$ is the bulk drag coefficient at z_m.

[38] For the parameterization of B_H^{-1} over a uniform land cover surfaces are generally classified as smooth, bluff-rough, or permeable-rough. Formulations have been derived experimentally and/or theoretically [*Brutsaert*, 1982; *Garratt*, 1992; *Verhoef et al.*, 1997; *Kustas and Norman*, 1999; *Massman*, 1999], often linking B_H^{-1} to the roughness Reynolds number z_{0+} $(=u_* z_{om}/\upsilon$, where z_{om} is the roughness length for momentum, and υ is the cinematic viscosity) through (at a given Prandtl number)

$$B_H^{-1} = a z_{0+}^{n_B} + b \tag{11}$$

with a, b and n_B being empirical coefficients. In Figure 6 the B_H^{-1} (z_{0+}) relationships of bare soil (i.e., bluff-rough), grass

and Aspen forest surfaces from *Brutsaert* [1982, Figure 4.24] are shown, and in Table 1 the corresponding values of a, b and n_B are reported. However, most natural surfaces are intermediate or composite thereby falling between these classes (for example in sparse or open canopies). For these surfaces, *Massman* [1999] developed a complex model, which provides estimates of B_H^{-1} as a function of LAI and canopy drag coefficient, but it requires detailed information (e.g., the vertical foliage distribution) that is not readily available. Instead, we examine two different approaches for estimating B_H^{-1}.

[39] 1. The land cover is viewed as a set of tiles of WV and NWV. Within each component tile, the surface roughness (and interfacial properties) are assumed to be statistically homogeneous and representative of the cover type only in the tile (no dependency on neighbors). We refer to this as the "two-source tile model" (2ST) because the heat sources of WV and NWV are separately resolved, and the bulk heat transfer coefficient is computed as if the land cover is decomposed into two spatially homogeneous tiles.

[40] 2. The surface roughness and heat source elements are randomly distributed and sensed by the turbulent flow as a single 'hypothetical' surface. Hence the interfacial transfer properties appear to resemble those of a bluff rough surface (e.g., bare soil) with trees and shrubs adding "excess" roughness. We refer to this as the "two-source random model" (2SR), because the heat sources of WV and NWV are treated separately, but the bulk heat transfer coefficient is computed as spatially homogeneous.

[41] While in the 2ST approach, B_H^{-1} is evaluated by (11) using literature parameter values, in the 2SR approach we need to compute the spatially aggregated (effective) B_H^{-1} as a function of the spatially aggregated z_{0+} for the mixed WV-bare soil (P1 period) and WV-grass (P2 period) systems. Considering an analogous expression of (9) for the whole system, inverting it, and making explicit B_H^{-1} from (10) we estimate B_H^{-1} as

$$B_H^{-1} = Cd_m^{-0.5}\left(\frac{Cd_m \rho c_p u\left(\hat{T}_{s,fp} - T_a\right)}{H_{obs}} - 1\right) \tag{12}$$

where H_{obs} is the observed sensible heat flux, and $\hat{T}_{s,fp}$ is an estimated average value of the T_s of the whole ecosystem, weighted by the foot print model using an analogous equation of (6) for T_s. Then, we propose to define new relationships for B_H^{-1} (z_{0+}) for mixed land cover systems, fitting (11) to the scattered points estimated by (12), and therefore estimating the a, b and n_B coefficients of (11) for the two observation periods. This is done in section 4.1.

3.2.3. Latent Heat Flux

[42] For estimating the latent heat flux contribution of the kth cover type ($\hat{S}_{LE,k}$) the same methodology of $\hat{S}_{H,k}$ may be used, estimating $\hat{S}_{LE,k}$ from the difference between the land cover surface humidity of each kth cover type ($q_{s,k}$) and the air humidity [e.g., *Garratt*, 1992, equation 3.51], but much of the problem is the determination of the $q_{s,k}$. Indeed, for a saturated soil, wet canopy or water surface, $q_{s,k}$ equals the saturated value at that surface temperature, but for an unsaturated or drying surface, $q_{s,k}$ is not so readily determined [*Garratt*, 1992].

[43] For this reason, we propose to bypass this difficulty and estimate $\hat{S}_{LE,k}$ as a residual term of the energy budget.

Table 1. Estimates of the Interfacial Transfer Parameters for Several Surfaces Expressed as $B_H^{-1} = a\, z_{0+}^{nB} + b$ for a Prandtl Number Equal 0.71

Source	Surface Description	a	n_B	b	z_{o+}
Brutsaert [1982]	bluff-rough surface	6.15	0.25	−5	10^0–10^3
Brutsaert [1982]	grass	1.46	0.23	0	10^2–10^3
Brutsaert [1982]	aspen forest	3×10^{-5}	1	0.2	10^4–10^5
Estimated	grass-WV	0.117	0.53	0	10^3–10^5
Estimated	soil-WV	0.034	0.59	0	10^3–10^5

For obtaining a more robust estimate we compute the latent heat flux at the daily timescale, as is appropriate for hydrologic balance calculations. A successful technique for daily averaging the energy flux is based on the assumption of the self-preservation of the evaporative fraction of the kth cover type (EF_k), which is the ratio of the latent energy flux to the available energy [*Crago and Brutsaert*, 1996]. We assume that EF_k is constant during the daylight hours (i.e., when $\hat{S}_{Qn,k} > 0$), and the best estimate of EF_k is taken from the middle of the day (e.g., between 10:00 and 16:30). In this way EF_k can be computed by

$$EF_k = \frac{1}{n_{md}} \sum_{l=1}^{n_{md}} \frac{\hat{S}_{LE,kl}}{\hat{S}_{Qn,kl}} = \frac{1}{n_{md}} \sum_{l=1}^{n_{md}} \frac{\hat{S}_{Qn,kl} - \hat{S}_{H,kl}}{\hat{S}_{Qn,kl}} \tag{13}$$

where n_{md} is the number of time steps included in the middle of the day computations, and the daily latent heat flux contribution of the kth cover type ($\hat{S}_{LEd,k}$) is estimated as

$$\hat{S}_{LEd,k} = EF_k \frac{1}{n_d} \sum_{t=1}^{n_d} \hat{S}_{Qn,kt} \tag{14}$$

where n_d is the number of time steps included in the daylight computations ($\hat{S}_{Qn,k} > 0$).

3.3. Comparison Between Predictions and Tower-Based Observations of the Energy Fluxes

[44] The $\hat{S}_k$ energy flux contributions are predicted by (7)–(14) using $R_{sw,in}$, $R_{lw,in}$, $T_{s,k}$, u, and T_a measurements, and scaled by the footprint weights for comparison with tower measurements. For LE and H we compare the predicted fluxes with adjusted eddy correlation measurements (LE_{obs} and H_{obs}) that have been rescaled to force energy balance closure [*Blanken et al.*, 1997; *Twine et al.*, 2000]. This method assumes that the Bowen ratio ($Bo = H_{obs}/\mathrm{LE}_{obs}$) is measured accurately by the eddy correlation system, and observed H and LE are adjusted to preserve the Bo and conserve the energy [*Blanken et al.*, 1997], so that the fluxes are estimated by:

$$\mathrm{LE}_{obs} = \frac{\hat{Q}_{n,ec}}{1 + Bo}; \quad H_{obs} = Bo\, \mathrm{LE}_{obs} \tag{15}$$

where $\hat{Q}_{n,ec}$ is the recalculated available energy by (6) with the eddy correlation footprint.

3.4. The β Function

[45] For estimating hydrologic relationships between θ and the evapotranspiration of each land cover type, we compute the β function defined as the ratio between the

Table 2. Radiative and Soil Heat Flux Dimensionless Parameter Values for Each Land Cover: Surface Albedo (α), Surface Emissivity (ε), and Fraction of Soil Heat Flux to Net Radiation (c)[a]

Land Cover	α_s	c	ε
Soil	0.15 [0.1–0.35]	0.21 [0.1–0.3]	0.97 [0.95–0.98]
WV	0.08 [0.07–0.2]	0.04	0.98 [0.96–0.97]
Grass	0.16 [0.15–0.30]	0.14	0.97 [0.97–0.98]
Mix	0.12	0.13	0.97

[a]Reported ranges from the literature [*Brutsaert*, 1982; *Garratt*, 1992; *Brutsaert*, 2005] are shown in brackets.

evapotranspiration and the potential evapotranspiration of the kth cover type. The evapotranspiration contribution of the kth cover type is estimated through (14), converting $\hat{S}_{LEd,k}$ in units of water loss per day (i.e., dividing $\hat{S}_{LEd,k}$ per the latent heat of vaporization and the water density), and the potential evapotranspiration is estimated through the Priestley-Taylor equation [e.g., *Brutsaert*, 1982, equation (10.23)], with the α_e Priestley-Taylor coefficient assumed equal to 1.26. In this way, β can be computed for each kth cover type at daily timescale during both the two observation periods (P1 and P2), and using both the two approaches (2SR and 2ST) described in section 3.2.2.

4. Results and Discussion

[46] First, the B_H^{-1} (z_{0+}) relationships necessary for the 2SR approach are estimated through (11) and (12). Then, the performance of the two approaches in predicting energy fluxes is evaluated. Finally, the β functions for the cover types are estimated and their ecohydrologic significance is discussed.

4.1. Estimate of Interfacial and Surface Roughness Properties

[47] For the 2SR approach we need to estimate B_H^{-1} through (12). First, $F_{fp,k}$ time series of the micrometeorological observations are estimated using (4) and (B2). Figure 3c reports the frequency distribution of the fraction of the WV cover in the footprint of the micrometeorological observations ($F_{fp,WV}$) for the entire data set. We note that $F_{fp,WV}$ is mainly in the range of 0.1–0.22 with the peak of the distribution close to 0.15. Average diurnal courses of $\hat{T}_{s,fp}$ for each of the two periods are plotted in Figure 4.

[48] In Figure 6 the computed B_H^{-1} values are plotted versus z_{0+} values for the composite WV-bare soil (points) and WV-grass (circles) surfaces [*Brutsaert*, 1982, Figure 4.24]. The B_H^{-1} (z_{o+}) functions of type (11) are fitted to the observed values for the two composite surfaces, and the a, b and n_B coefficients of (11) are computed (Table 1). Functionally, the rapid increase in effective B_H^{-1} with increasing z_{0+} resembles a bluff-rough surface but with a z_{0+} much larger than those reported for bare soil (or grass) alone (see Table 1). The dependence of the effective B_H^{-1} on z_{0+} is also much stronger than those reported for strictly grass or WV (Figure 6).

[49] For the 2ST approach, we assume a constant value of B_H^{-1} (=2) for WV due to its low variability with z_{0+} (c.f. Aspen forest in Figure 6), and use literature values for the a, b and n_B coefficients of (11) for grass and bare soil (Table 1). Using these interfacial transfer model parameters, we optimized z_{om} for bare soil and grass to best match (in a root-mean-square sense) H_{obs}. This optimization resulted in a bare soil $z_{om} \approx 0.015$ m, which is close to the literature values (0.001–0.01 m [*Garratt*, 1992]). For grass, the optimization yielded a $z_{om} \approx 0.05$ m, also consistent with literature values and the rule of thumb relating canopy height h_c ($\approx$0.5 m) to z_{om} ($z_{om}/h_c \approx 0.1$ [*Garratt*, 1992]).

4.2. Calibration of the Models

[50] The comparison between predicted and observed energy flux is made at the daily timescale and in units of mm/d of water for better assessing the impact on the soil water balance. The fraction of WV cover of the radiometer footprint is 0.38. The values of α_k of each land cover type were adjusted starting from literature values [e.g., *Brutsaert*, 1982; *Garratt*, 1992; *Brutsaert*, 2005], to best match (in a root-mean-square sense) the observed values of the reflected shortwave radiation (Table 2). The values of ε_k were chosen from literature values [e.g., *Brutsaert*, 1982; *Garratt*, 1992] (Table 2) to best match longwave radiation observations using the IRTS-P observations of $T_{s,k}$. However, the emissivity is implicit in the IRTS-P design and it is fairly insensitive to modest variations in vegetation type [*Bugbee et al.*, 1998]. Predicted net radiation obtained from (6) with $\hat{S}_{Rn,k}$ given by (7) match very well the observations for both the two observation periods (Table 3).

[51] The availability of soil heat flux probes for both the NWV and WV cover types allowed for the calibration of the c_k parameters of (8) (Table 2), obtaining very low root-mean-square errors (RMSE) (RMSE $\approx$ 0.16 mm/d for bare soil and grass components and even lower for the WV component). Hence the available energy is well predicted.

[52] The energy balance closure of observed surface flux is successfully tested comparing the observed LE + H and the $\hat{Q}_{n,ec}$ recalculated available energy with the eddy correlation footprint. For P1 LE + H is overestimated by approximately 5% relative to $\hat{Q}_{n,ec}$, and for P2 it is underestimated by 5% using the surface fluxes not rescaled to force energy balance closure.

[53] We indicate with $\hat{Z}_H$ and $Z_{H,obs}$ predicted and observed sensible heat fluxes expressed in mm/d of water. Comparisons between measured and modeled (using both

Table 3. Comparison Between Observed and Modeled Fluxes[a]

Model	Period	ω_1	ω_2, mm/d of water	r^2	RMSE, mm/d of water
$\hat{Z}_{Rn}$	I	0.95	0.06	0.99	0.22
$\hat{Z}_{Rn}$	II	1	−0.01	1.00	0.08
$\hat{Z}_{H,2\text{-}ST}$	I	1.22	−0.48	0.82	0.61
$\hat{Z}_{H,2\text{-}SR}$	I	0.95	0.22	0.77	0.40
$\hat{Z}_{H,2\text{-}ST}$	II	1.08	−0.03	0.70	0.74
$\hat{Z}_{H,2\text{-}SR}$	II	0.91	0.12	0.78	0.50
$\hat{E}T_{2\text{-}ST}$	I	0.89	0.24	0.67	0.33
$\hat{E}T_{2\text{-}SR}$	I	0.76	0.47	0.64	0.39
$\hat{E}T_{2\text{-}ST}$	II	1.08	−0.41	0.68	0.68
$\hat{E}T_{2\text{-}SR}$	II	1.11	−0.23	0.75	0.58

[a]Net radiation is indicated with $\hat{Z}_{Rn}$, and the sensible heat flux is indicated with $\hat{Z}_H$. The comparison is conducted via a regression model of the form $y = \omega_1 x + \omega_2$, where y is the modeled flux and x is the observed flux. The coefficient of determination (r^2), and the root-mean-square error (RMSE) are shown. The indexes "I" and "II" refer to the P1 soil-WV and P2 grass-WV periods, respectively.

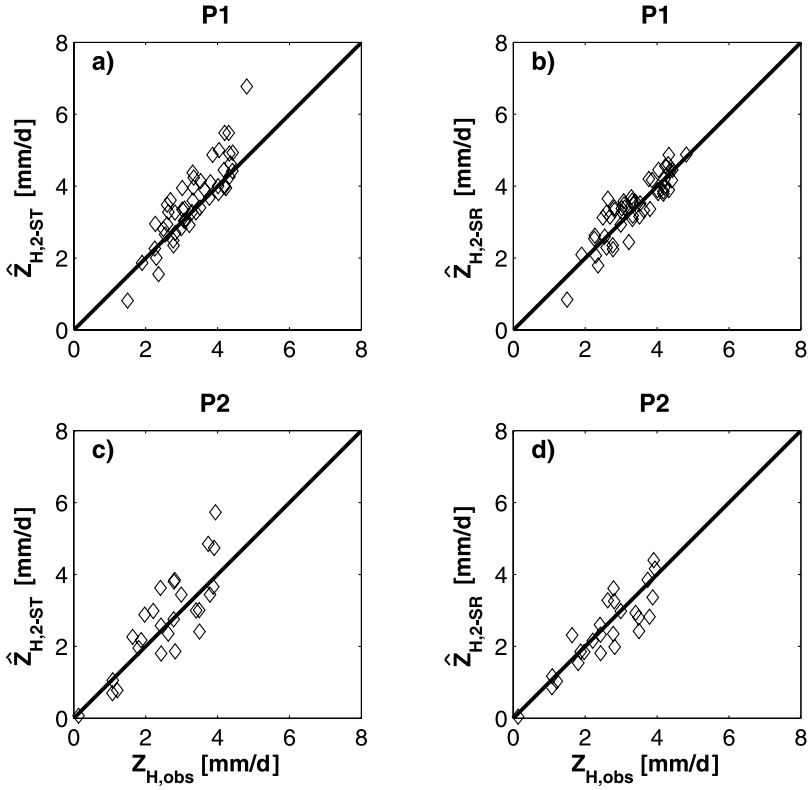

Figure 7. Comparison between observed ($Z_{H,obs}$) and modeled (using both the 2ST and the 2SR approaches) daytime sensible heat flux for (a and b) P1 and (c and d) P2. The 1:1 line is shown for reference.

2ST and 2SR approaches) sensible heat flux are shown in Figure 7, and Table 3 reports statistics of comparison. In P1 $Z_{H,obs}$ is fairly well reproduced using both approaches (RMSE $\leq$ 0.61 mm/d); however, the overall performance of 2SR in terms of near-unity of the regression slope and RMSE are slightly better than 2ST. In the spring time (P2), the correlation coefficients and RMSE values (Table 3) are mildly degraded though the difference in performance is not statistically significant (Figure 7 and Table 3).

[54] The assumption of the self preservation of the evaporative fraction was verified, with the data showing this ratio to be nearly constant from 10:00 to 16:30. Hence the latent heat flux can be estimated trough (14) and (6). Predicted ET (using both 2ST and 2SR approaches) are compared to observed ET in Figure 8 and Table 3. In contrast with the sensible heat flux, similar predictions of the latent heat flux are obtained for both the 2SR and 2ST approaches for P1 (RMSE $\leq$ 0.39 mm/d). For P2 the agreement between measured and modeled ET becomes worse (RMSE $\leq$ 0.68 mm/d), which is contributed to by the degraded $\hat{Z}_H$ predictions during this period. We note that these RMSE predictions are very close to RMSE values (=0.5 mm/d) reported for daily bare soil evaporation using skin temperature measurements for input and lysimeter ET measurements for model validation [*Katul and Parlange*, 1992].

[55] To assess the impact of the difference in $\hat{\text{ET}}$ predictions over a long period, we compute the cumulative modeled and observed ET, and the modeled potential evapotranspiration (PET) for the two periods (Figure 9). In P1 the total observed evapotranspiration (ET_{obs}) is well predicted by 2ST (difference of less than 10%), while it is moderately overestimated by 2SR (difference of $\sim$20%). In P2 both approaches provide accurate estimates of the total ET, with difference between observed and modeled being less than 8 %. Hence, since the observed and modeled ET rates are similar at half-hourly timescales and when integrated to express the total impact to the surface water balance, we conclude that the proposed approach for estimating ET performs well.

4.3. Sensitivity Analysis of the Evapotranspiration to the Fraction of Vegetation Cover

[56] In section 2.3 we highlighted the heterogeneity of the field showing that $\frac{\text{NDVI}}{\text{NDVI}_{\text{MAX}}}$, which represents the average value of the fraction of WV cover of the field ($F_{c,WV}$) as assumed in § 3.2, varies between 0.1 and 0.4 with the size and relative direction of the area being averaged cover. Instead, using the flux footprint model, the $F_{fp,WV}$ of the eddy correlation observations tends to stay in the range 0.1–0.22.

[57] For highlighting the impact on $\hat{\text{ET}}$ of potential errors in specifying the correct value of the fraction of the land cover type, and for demonstrating the importance of the use of the footprint model in the interpretation of observations of ET in heterogeneous terrain we perform a sensitivity analysis of ET to $F_{c,WV}$.

[58] We vary $F_{c,WV}$ in the range 0.0–0.4, and model the energy flux with two approaches commonly implemented in LSMs [e.g., *Noilhan and Planton*, 1989; *Koster and Suarez*, 1992; *Giorgi and Avissar*, 1997; *Albertson and Kiely*, 2001;

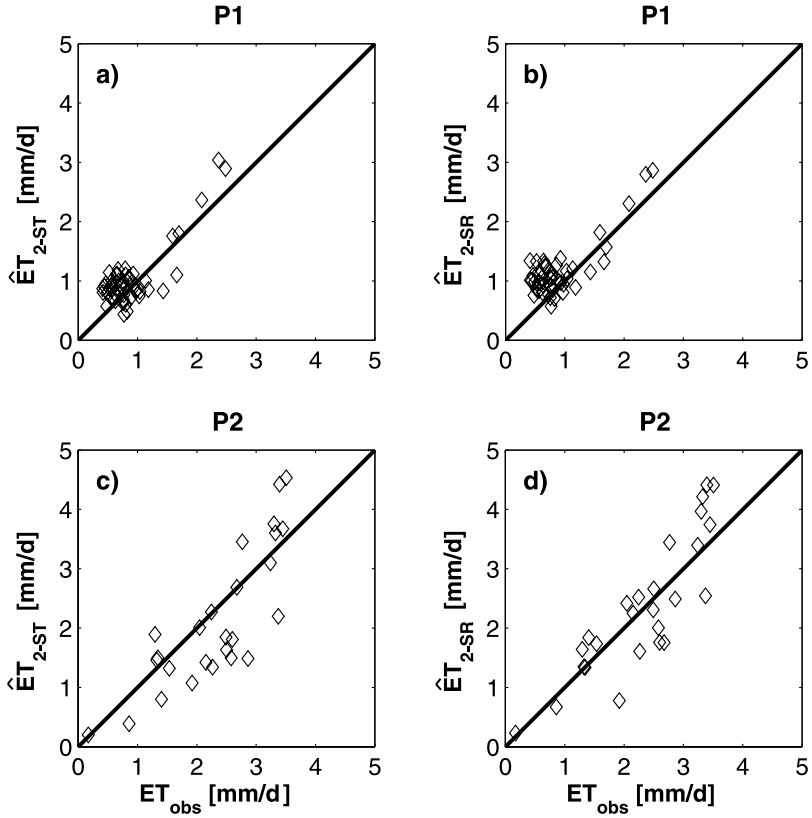

Figure 8. Same as Figure 7, but for evapotranspiration.

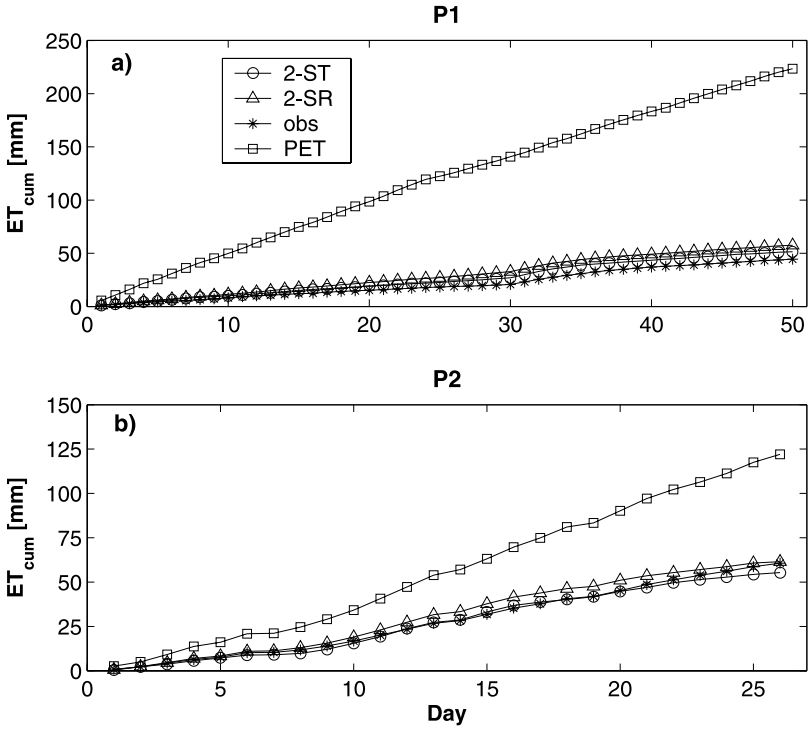

Figure 9. Cumulative observed (ET_{obs}) and modeled (both 2ST and 2SR) ET during (a) P1 and (b) P2. Here the abscissa "Day" represents sequential days excluding precipitation and gaps. The PET is estimated using the Priestley-Taylor equation.

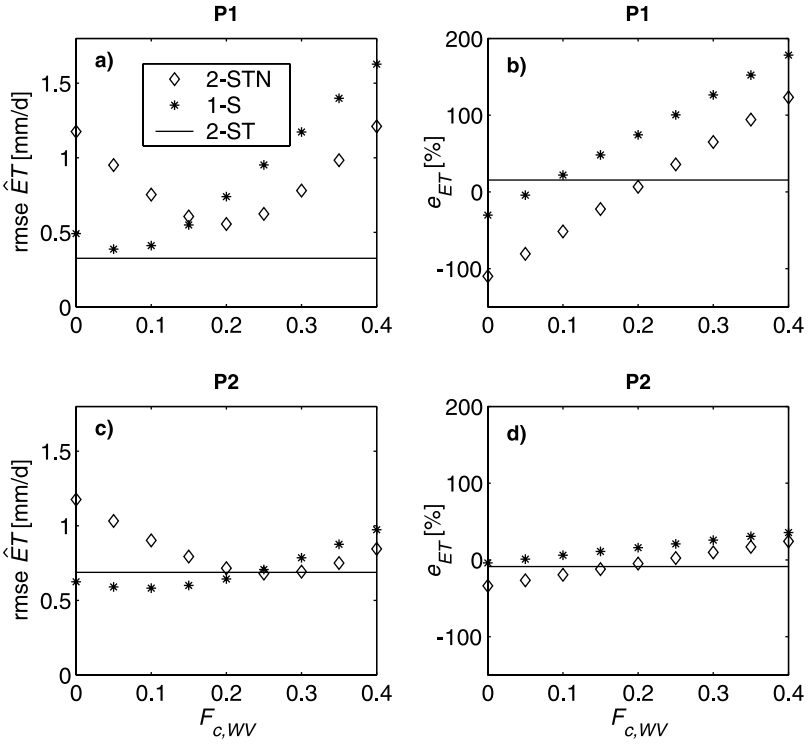

Figure 10. (a and c) RMSE of ET and (b and d) e_{ET} predicted by 2STN and 1S across the range of $F_{c,WV}$ for the two periods. For reference the RMSE and e_{ET} using the 2ST is also plotted (solid line).

Montaldo and Albertson, 2001]: (1) a two-tile approach without the foot print model (2STN) and (2) a lumped approach, also without the foot print model (1S). In particular, fluxes are predicted using (1) 2STN, which is equation (6) with a constant value of $F_{fp,k}$; since $n_e = 2$ in this case, the constant values of the fraction of land covers are $F_{c,WV}$ and $1 - F_{c,WV}$, respectively, and (2) 1S, which is equations (7), (8), (9), and (14) but implemented for the whole system. Hence we estimated lumped values of α, ε and c from literature values (Table 2), and a mixed value of $\hat{T}_{s,mix}$ [$=T_{s,WV}\,F_{c,WV} + T_{s,NWV}\,(1 - F_{c,WV})$, with $T_{s,WV}$ and $T_{s,NWV}$ the surface temperatures of the WV and NWV, respectively], and use the spatially aggregated B_H^{-1} estimated previously (see section 4.1) and shown in Figure 6.

[59] For the two periods and across the range of $F_{c,WV}$, Figure 10 shows the RMSE of ET and the error of the total ET (e_{ET}) defined as

$$e_{\mathrm{ET}} = \frac{\hat{\mathrm{ET}}_T - \mathrm{ET}_{obs,T}}{\mathrm{ET}_{obs,T}} \tag{16}$$

where $\hat{\mathrm{ET}}_T$ and $\mathrm{ET}_{obs,T}$ are the predicted and observed total ET for the whole period, respectively. For comparison the reference values using the 2ST are also plotted (solid lines). From Figure 10a we note that in P1 the RMSE of 2STN varies between 0.55 mm/d and 1.21 mm/d, and the RMSE of 1S varies even more, between 0.39 and 1.63, but never reaching the low value of RMSE of 2ST. The impact on the total evapotranspiration is large (Figure 10b) with variation of e_{LE} of more than 200% for both 2STN and 1S across the range of $F_{c,WV}$ values. Hence ET is significantly sensitive to $F_{c,WV}$ during the P1 characterized by the two highly contrasting land cover types (bare soil and WV), and potential errors of $F_{c,WV}$ can impact the total ET and, consequently, the soil water balance of this water-limited ecosystem.

[60] Instead, less sensitivity of ET to $F_{c,WV}$ is found for P2 (Figures 10c and 10d), because bare soil is not present and surface thermal states of grasses and WV are more similar (Figure 4).

4.4. Estimates of the β Functions

[61] The daytime β of each land cover component is computed across the range of θ for both periods (Figure 11). We note the following.

[62] 1. The β of WV (β_{WV}) appears insensitive to large variations in θ for both periods, at least when compared to the soil and grasses. This is not surprising as the typical shrubs and trees of Mediterranean water-limited ecosystems are known to be highly tolerant to water content fluctuations and are usually slower to limit their water losses when compared to grasses [*Larcher*, 1995]. For instance, literature values indicate that the *Olea* can tolerate leaf water potentials as extreme as -2 to -3 MPa [*Lo Gullo et al.*, 2003] and -6 MPa [*Sakcali and Ozturk*, 2004], and the types of *Quercus* in these regions can tolerate -2.5 to -6 MPa [*Tognetti et al.*, 1998; *Sakcali and Ozturk*, 2004] without significant drop of leaf conductance, while minimal water potential values of these resistant shrubs may reach -8 MPa [*Larcher*, 1995]. These potentials correspond to extremely low values of θ (0.07–0.08), such as estimated by the *van Genuchten*'s [1980] soil retention curve using the pedotransfer function of *Carsel and Parrish* [1988]. For this reason, the WV system did not experience excessive soil moisture stress, and the values of the β_{WV} never fell below 0.6 using 2ST or 0.8 using 2SR even for the dry

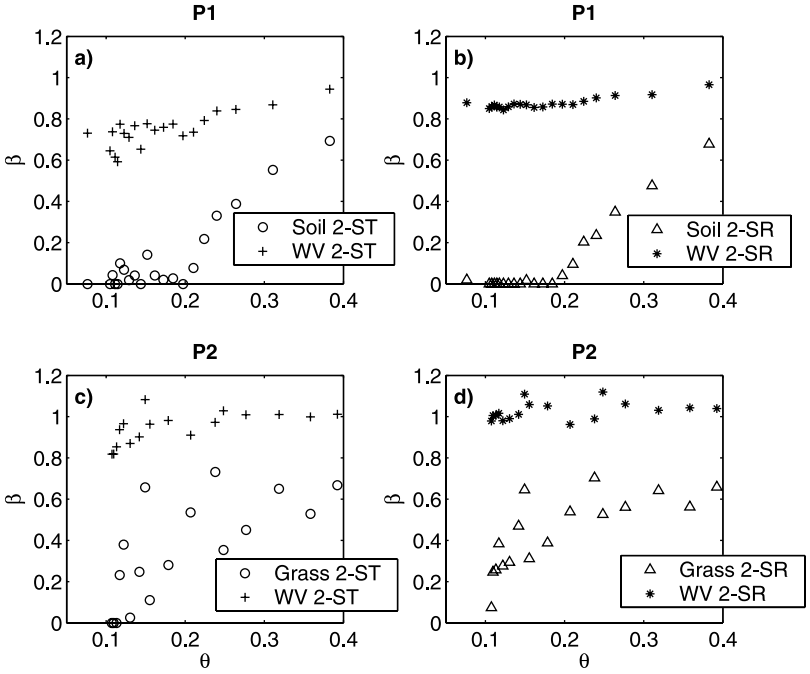

Figure 11. Daytime β of each land cover component across the range of θ for (a and b) P1 and (c and d) P2 and both the modeling approaches (2ST and 2SR).

conditions of the summer 2003, which was one of the driest in the last decades in Sardinia.

[63] 2. The grass β function (β_g) suggests a wilting point of $\theta \sim 0.1$, and a commencement of transpiration reduction below about 0.2. Note that for high θ values the β_g doesn't reach a value of 1 because other environmental factors (e.g., temperature, vapor pressure deficit and photosynthetically active radiation may be suboptimal for these grasses) are stressing the plant and increasing the canopy resistance [e.g., *Larcher*, 1995; *Montaldo et al.*, 2005].

[64] 3. During P1 the bare soil β function is close to 0 for θ values below about 0.18, and then increases nonlinearly for higher θ values as suggested by *Parlange et al.* [1999], contrasting significantly with β_{WV}.

5. Conclusion

[65] The use of a 2-D footprint model, ground based thermal infrared observations and high resolution remote sensing images (in conjunction with measurements of wind velocity, air temperature and incoming shortwave and longwave radiation) provides flux estimates that match well the tower-based observed energy fluxes. For the purposes of estimating sensible heat flux the use of a proposed two-source random model (2SR), which treats the heat sources of WV and NWV separately but computes the bulk heat transfer coefficient as spatially homogeneous, allows slightly better performance than the use of the common two-source tile model (2ST) approach. For implementing the 2SR approach new relationships between the B_H^{-1} interfacial transfer coefficient and z_{0+} are estimated for the two composite surfaces (bare soil-WV, and grass-WV) that characterize this Mediterranean ecosystem. The interfacial transfer coefficient resembles for both composite surfaces a bluff-rough surface but with increased momentum roughness length. In fact, the dependence of the effective B_H^{-1} on z_{0+} is much stronger (in this case of an open canopy) than those reported for either full grass or tree cover.

[66] We demonstrated the possibility to estimate accurately ET in heterogeneous ecosystems using surface temperature remote observations and high-resolution VIS/NIR remote sensing information. These results are particularly significant for remote sensing applications, when land surface fluxes over a region are estimated from land surface states monitored by remote sensing platforms (diagnostic perspective).

[67] Moreover, the sensitivity analysis of modeled ET to the fraction of WV cover ($F_{c,WV}$) in this heterogeneous ecosystem demonstrates (1) the importance of using a footprint model for interpreting micrometeorological observations and (2) the strong impact of $F_{c,WV}$ potential errors on the water loss for evapotranspiration and, consequently, on the soil water balance of this water-limited ecosystem in the summer.

[68] Using the proposed approaches we also estimate the relationships between soil water content and ET for each land cover component successfully. The typical WV species of Sardinia, representative of the broader Mediterranean water-limited region, confirm a strong tolerance to prolonged drought, such as occurred in the summer of 2003 (as part of a long-term drought on the island that created a water resources management crisis). Even with the extreme dry conditions the WV species were still transpiring at rates close to potential. Instead, the grass is less tolerant to water content fluctuations, transpires at lower rates than WV, and wilts as the dry summer season commences. The β values of the bare soil component are much lower compared to WV and grass β values for dry soil conditions. The switch from grass to bare soil has a significant impact on increasing the sensitivity of the bulk ecosystem ET to θ during the summer. Hence we demonstrated that the ET rates of the

three main landscape components significantly differ for limiting θ values.

[69] These results need to be carefully considered in water resources and land use planning, because land cover changes (i.e., changes of fraction of PFT covers) may impact on the soil water losses through ET, and therefore on the water resources availability of these water-limited regions.

Appendix A: Orientation of the Eddy Correlation Sensors in Complex Terrain

[70] In a coordinate system (x, y, z) the three velocity components are defined as u, v and w. Over a sloping planar surface, the velocity components u and w should be taken parallel and normal to this surface, respectively. If the axis of the sonic anemometer is not orientated parallel to this surface then part of the horizontal velocity is recorded as vertical velocity (with significant implications to the scalar fluxes). The effective slope varies with topography and hence with the wind direction. Such a slope can be evaluated using a digital elevation model (DEM) map for one direction only or a regression between the horizontal angle $\chi_o = \tan^{-1}\left(\frac{\overline{v}}{\overline{u}}\right)$ and the vertical angle $\chi_v = \tan^{-1}\left(\frac{\overline{w}}{\overline{u}}\right)$ if a long-term time series is available. The latter approach is adopted here. The relevant flow statistics in the transformed coordinates can be derived from the original sonic anemometer coordinate (shown in capital letters for clarity) system using:
means:

$$\begin{aligned}\overline{u} &= A_1A_3\overline{U} + A_2A_3\overline{V} + A_4\overline{W}\\ \overline{v} &= 0\\ \overline{w} &= -A_1A_4\overline{U} - A_2A_4\overline{V} + A_3\overline{W}\end{aligned} \tag{A1}$$

variances:

$$\begin{aligned}\overline{u'^2} &= A_3^2\left(A_1^2\overline{U'^2} + A_2^2\overline{V'^2} + 2A_1A_2\overline{U'V'}\right) + A_4^2\overline{W'^2} + 2A_3A_4\\ &\quad\cdot\left(A_1\overline{W'U'} + A_2\overline{W'V'}\right)\\ \overline{v'^2} &= A_1^2\overline{V'^2} + A_2^2\overline{U'^2} + 2A_1A_2\overline{U'W'}\\ \overline{w'^2} &= A_4^2\left(A_1^2\overline{U'^2} + A_2^2\overline{V'^2}\right) + A_3^2\overline{W'^2} - 2A_3A_4\\ &\quad\cdot\left(A_1\overline{W'U'} + A_2\overline{W'V'} + A_1A_2\overline{U'V'}\right)\end{aligned} \tag{A2}$$

stresses:

$$\begin{aligned}\overline{u'v'} &= \left(A_1^2 - A_2^2\right)A_3\overline{U'V'} - A_1A_2\overline{U'^2} + A_1A_2A_3\overline{V'^2} + A_1A_4\overline{W'V'}\\ &\quad - A_2A_4\overline{W'U'}\\ \overline{u'w'} &= \left(A_1A_3^2 - A_1A_4^2\right)\overline{U'W'} - A_1^2A_3A_4\overline{U'^2} - 2A_1A_2A_3A_4\overline{U'V'}\\ &\quad + \left(A_2A_3^2 - A_2A_4^2\right)\overline{W'V'} - A_2^2A_3A_4\overline{V'^2} + A_3A_4\overline{W'^2}\\ \overline{u'v'} &= \left(A_1^2 - A_2^2\right)A_3\overline{U'V'} - A_1A_2\overline{U'^2} + A_1A_2A_3\overline{v'^2} + A_1A_4\overline{W'V'}\\ &\quad - A_2A_4\overline{W'U'}\end{aligned} \tag{A3}$$

scalar fluxes, Φ:

$$\overline{w'\Phi'} = A_3\overline{W'\Phi'} - A_1A_4\overline{U'\Phi'} - A_2A_4\overline{V'\Phi'} \tag{A4}$$

where $A_1 = \cos\chi_o$, $A_2 = \sin\chi_o$, $A_3 = \cos\chi_v$, $A_4 = \sin\chi_v$. In the manuscript, we used small-case letters as already transformed variables for consistency with the literature.

Appendix B: Extension of the H2000 Footprint Model of *Hsieh et al.* [2000] to Two Dimensions

[71] The basic equation of the H2000 model and its extension to 2-D are discussed here. The cross-wind integrated footprint

$$F^y = \frac{1}{k_v^2x^2}Dz_u^P|L|^{1-P}e^{\frac{Dz_u^P|L|^{1-P}}{k_v^2x}} \tag{B1}$$

where z_u is the length scale of H2000, L is the Obukhov's length [*Brutsaert*, 1982], k_v (=0.4) is the von Karman's constant, D and P are similarity constants which values change for unstable, neutral and stable atmospheric conditions [*Hsieh et al.*, 2000].

[72] Because this model predicts only the cross-wind integrated footprint, the contribution of lateral dispersion must be added to generate a 2-D source area function. Starting from the assumption that diffusion in the vertical and crosswind direction can be treated independently, f can be estimated through

$$f(x,y,z_m) = D_y(x,y)F^y(x,z_m) \tag{B2}$$

where D_y is the lateral diffusion and is commonly assumed to be Gaussian [*Schmid*, 1994], so that it can be estimated as:

$$D_y(x,y) = \frac{1}{\sqrt{2\pi}\sigma_y}e^{-\frac{1}{2}\left(\frac{y}{\sigma_y}\right)^2} \tag{B3}$$

where the standard deviation σ_y can be related to the standard deviation in the lateral wind fluctuations, σ_v as [*Eckman*, 1994]:

$$\sigma_y = a_1z_{om}\frac{\sigma_v}{u_*}\left(\frac{x}{z_{om}}\right)^{p_1} \tag{B4}$$

where u_* is the friction velocity, z_{om} is the roughness length for momentum, and a_1 (=0.3) and p_1 (=0.86) are similarity parameters.

[73] **Acknowledgments.** The participation of M. Detto, M. Mancini, and N. Montaldo in this research was supported by the Ministero dell'Università e della Ricerca Scientifica e tecnologica of Italy through grant 2002084552_003 and the Istituto Nazionale della montagna (Agenzia 2002). The participation of J. D. Albertson and G. Katul in this research was supported by the Office of Science (BER), U.S. Department of Energy (grants DE-FG02-00ER63015 and DE-FC02-03ER63613) and the National Science Foundation (NSF-EAR 0208258). We thank Paolo Botti, Maria Antonietta Dessena, and Gianni Borghero of the Ente Autonomo del Flumendosa (Cagliari, Italy) for the support in the tower setup and maintenance. Finally, we thank the three anonymous reviewers and Nelson Dias for their useful comments.

References

Albertson, J. D., and G. Kiely (2001), On the structure of soil moisture time series in the context of land surface models, *J. Hydrol.*, *243*(1–2), 101–119.

Albertson, J. D., and N. Montaldo (2003), Temporal dynamics of soil moisture variability: 1. Theoretical basis, *Water Resour. Res.*, *39*(10), 1274, doi:10.1029/2002WR001616.

Altese, E., O. Bolognani, M. Mancini, and P. A. Troch (1996), Retrieving soil moisture over bare soil from ERS-1 synthetic aperture radar data: Sensitivity analysis based on a theoretical surface scattering model and field data, *Water Resour. Res.*, *32*(3), 653–661.

Baldocchi, D., and S. Rao (1995), Intra-field variability of scalar flux densities across a transition between a desert and an irrigated potato site, *Boundary Layer Meteorol.*, *76*, 109–136.

Baldocchi, D., J. Finnigan, K. Wilson, K. T. U. Paw, and E. Falge (2000), On measuring net ecosystem carbon exchange over tall vegetation on complex terrain, *Boundary Layer Meteorol.*, *96*(1–2), 257–291.

Baldocchi, D. D., L. Xu, and N. Kiang (2004), How plant functional-type, weather, seasonal drought, and soil physical properties alter water and energy fluxes of an oak-grass savanna and an annual grassland, *Agric. Forest. Meteorol.*, *123*, 13–39.

Blanken, P. D., T. A. Black, P. C. Yang, H. H. Neumann, Z. Nesic, R. Staebler, G. den Hartog, M. D. Novak, and X. Lee (1997), Energy balance and canopy conductance of a boreal aspen forest: Partitioning overstory and understory components, *J. Geophys. Res.*, *102*(D24), 28,915–28,927.

Brunetti, M., M. Maugeri, T. Nanni, and A. Navarra (2002), Droughts and extreme events in regional daily Italian precipitation series, *Int. J. Climatol.*, *22*, 543–558.

Brutsaert, W. (1982), *Evaporation Into the Atmosphere*, 299 pp., Springer, New York.

Brutsaert, W. (2005), *Hydrology: An Introduction*, 605 pp., Cambridge Univ. Press, New York.

Bugbee, B., M. Droter, O. Monje, and B. Tanner (1998), Evaluation and modification of commercial infra-red transducers for leaf temperature measurement, *Adv. Space Res.*, *22*(10), 1425–1434.

Caparrini, F., F. Castelli, and D. Entekhabi (2004), Estimation of surface turbulent fluxes through assimilation of radiometric surface temperature sequences, *J. Hydrometeorol.*, *5*(1), 145–159.

Carlson, T. N., and D. A. Ripley (1997), On the relation between NDVI, fractional vegetation cover, and leaf area index, *Remote Sens. Environ.*, *62*(3), 241–252.

Carsel, R. F., and R. S. Parrish (1988), Developing joint probability distributions of soil water retention characteristics, *Water Resour. Res.*, *24*(5), 755–769.

Ceballos, A., J. Martinez-Fernandez, and M. A. Luengo-Ugidos (2004), Analysis of rainfall trends and dry periods on a pluviometric gradient representative of Mediterranean climate in the Duero Basin, Spain, *J. Arid Environ.*, *58*(2), 215–233.

Crago, R., and W. Brutsaert (1996), Daytime evaporation and the self-preservation of the evaporative fraction and the Bowen ratio, *J. Hydrol.*, *178*(1–4), 241–255.

Dash, P., F. M. Gottsche, F. S. Olesen, and H. Fischer (2002), Land surface temperature and emissivity estimation from passive sensor data: Theory and practice-current trends, *Int. J. Remote Sens.*, *23*(13), 2563–2594.

Eckman, R. M. (1994), Re-examination of empirically derived formulas for horizontal diffusion from surface sources, *Atmos. Environ.*, *28*(2), 265–272.

Entekhabi, D., I. Rodriguez-Iturbe, and F. Castelli (1996), Mutual interaction of soil moisture state and atmospheric processes, *J. Hydrol.*, *184*, 3–17.

Entekhabi, D., et al. (2004), The hydrosphere state (Hydros) satellite mission: An Earth system pathfinder for global mapping of soil moisture and land freeze/thaw, *IEEE Trans. Geosci. Remote Sens.*, *42*(10), 2184–2195.

Fernandez, J. B. G., M. R. G. Mora, and F. G. Novo (2004), Vegetation dynamics of Mediterranean shrublands in former cultural landscape at Grazalema Mountains, south Spain, *Plant Ecol.*, *172*(1), 83–94.

Finnigan, J. (2004), The footprint concept in complex terrain, *Agric. For. Meteorol.*, *127*(3–4), 117–129.

Gamon, J. A., C. B. Field, M. L. Goulden, K. L. Griffin, A. E. Hartley, J. G. Penuelas, and R. Valentini (1995), Relationships between NDVI, canopy structure, and photosynthesis in 3 Californian vegetation types, *Ecol. Appl.*, *5*(1), 28–41.

Garratt, J. R. (1992), *The Atmospheric Boundary Layer*, Cambridge Univ. Press, New York.

Giorgi, F., and R. Avissar (1997), Representation of heterogeneity effects in earth system modeling: Experience from land surface modeling, *Rev. Geophys.*, *35*(4), 413–438.

Gutman, G., and A. Ignatov (1997), The derivation of the green vegetation fraction from NOAA/AVHRR data for use in numerical weather prediction models, *Int. J. Remote Sens.*, *19*(8), 1533–1543.

Halldin, S., S.-E. Gryningb, L. Gottschalkc, A. Jochumd, L.-C. Lundina, and A. A. Van de Griend (1999), Energy, water and carbon exchange in a boreal forest landscape—NOPEX experiences, *Agric. For. Meteorol.*, *98*(9), 5–29.

Holah, N., N. Baghdadi, M. Zribi, A. Bruand, and C. King (2005), Potential of ASAR/ENVISAT for the characterization of soil surface parameters over bare agricultural fields, *Remote Sens. Environ.*, *96*(1), 78–86.

Hsieh, C. I., G. Katul, and T. Chi (2000), An approximate analytical model for footprint estimation of scalar fluxes in thermally stratified atmospheric flows, *Adv. Water Resour.*, *23*(7), 765–772.

Jackson, R. B., J. L. Banner, E. G. Jobbágy, W. T. Pockman, and D. H. Wall (2002), Ecosystem carbon loss with woody plant invasion of grasslands, *Nature*, *418*, 623–626.

Jackson, T. J. (1997a), Soil moisture estimation using special satellite microwave/imager satellite data over a grassland region, *Water Resour. Res.*, *33*(6), 1475–1484.

Jackson, T. (1997b), Experiment plan: Southern Great Plains 1997 (SGP97) Hydrology Experiment, report, Hydrol. Lab., Agric. Res. Serv., Beltsville, Md.

Katul, G. G., and M. B. Parlange (1992), Estimation of bare soil evaporation using skin temperature measurements, *J. Hydrol.*, *132*, 91–106.

Kljun, N., P. Calanca, M. W. Rotachhi, and H. P. Schmid (2004), A simple parameterisation for flux footprint predictions, *Boundary Layer Meteorol.*, *112*(3), 503–523.

Koster, R. D., and M. J. Suarez (1992), Modeling the land surface boundary in climate models as a composite of independent vegetation stands, *J. Geophys. Res.*, *97*(D3), 2697–2715.

Kurc, S. A., and E. E. Small (2004), Dynamics of evapotranspiration in semiarid grassland and shrubland ecosystems during the summer monsoon season, central New Mexico, *Water Resour. Res.*, *40*, W09305, doi:10.1029/2004WR003068.

Kustas, W. P., and J. M. Norman (1999), Evaluation of soil and vegetation heat flux predictions using a simple two-source model with radiometric temperatures for partial canopy cover, *Agric. For. Meteorol.*, *94*(1), 13–29.

Kustas, W. P., J. H. Prueger, and L. E. Hipps (2002), Impact of using different time-averaged inputs for estimating sensible heat flux of riparian vegetation using radiometric surface temperature, *J. Appl. Meteorol.*, *41*(3), 319–332.

Kustas, W. P., J. M. Norman, M. C. Anderson, and A. N. French (2003), Estimating subpixel surface temperatures and energy fluxes from the vegetation index-radiometric temperature relationship, *Remote Sens. Environ.*, *85*(4), 429–440.

Larcher, W. (1995), *Physiological Plant Ecology*, Springer, New York.

Lelieveld, J., et al. (2002), Global air pollution crossroads over the Mediterranean, *Science*, *298*(5594), 794–799.

Lo Gullo, M. A., S. Salleo, R. Rosso, and P. Trifilo (2003), Drought resistance of 2-year-old saplings of Mediterranean forest trees in the field: Relations between water relations, hydraulics and productivity, *Plant Soil*, *250*(2), 259–272.

Mancini, M., R. Hoeben, and P. A. Troch (1999), Multifrequency radar observations of bare surface soil moisture content: A laboratory experiment, *Water Resour. Res.*, *35*(6), 1827–1838.

Maselli, F., M. Chiesi, and M. Bindi (2004), Multi-year simulation of Mediterranean forest transpiration by the integration of NOAA-AVHRR and ancillary data, *Int. J. Remote Sens.*, *25*(19), 3929–3941.

Massman, W. J. (1999), A model study of kB(H)(−1) for vegetated surfaces using "localized near-field" Lagrangian theory, *J. Hydrol.*, *223*(1–2), 27–43.

Montaldo, N., and J. D. Albertson (2001), On the use of the force-restore SVAT model formulation for stratified soils, *J. Hydrometeorol.*, *2*(6), 571–578.

Montaldo, N., J. D. Albertson, M. Mancini, and G. Kiely (2001), Robust simulation of root zone soil moisture with assimilation of surface soil moisture data, *Water Resour. Res.*, *37*(12), 2889–2900.

Montaldo, N., V. Toninelli, J. D. Albertson, M. Mancini, and P. A. Troch (2003), The effect of background hydrometeorological conditions on the sensitivity of evapotranspiration to model parameters: Analysis with measurements from an Italian alpine catchment, *Hydrol. Earth Syst. Sci.*, *7*(6), 848–861.

Montaldo, N., R. Rondena, J. D. Albertson, and M. Mancini (2005), Parsimonious modeling of vegetation dynamics for ecohydrologic studies of water-limited ecosystems, *Water Resour. Res.*, *41*, W10416, doi:10.1029/2005WR004094.

Moonen, A. C., L. Ercoli, M. Mariotti, and A. Masoni (2002), Climate change in Italy indicated by agrometeorological indices over 122 years, *Agric. For. Meteorol.*, *111*(1), 13–27.

Mouillot, F., S. Rambal, and R. Joffre (2002), Simulating climate change impacts on fire frequency and vegetation dynamics in a Mediterranean-type ecosystem, *Global Change Biol.*, *8*(5), 423–437.

Noilhan, J., and S. Planton (1989), A simple parameterization of land surface processes for meteorological models, *Mon. Weather Rev.*, *117*, 536–549.

Parlange, M. B., J. D. Albertson, W. E. Eichinger, A. T. Cahill, and T. J. Jackson (1999), Evaporation: Use of fast response turbulence sensors, Raman lidar and passive microwave remote sensing, in *Vadose Zone Hydrology: Cutting Across Disciplines*, edited by M. B. Parlange and J. W. Hopmans, pp. 260–278, Oxford Univ. Press, New York.

Ragab, R., D. Moidinis, J. Albergel, J. Khouri, A. Drubi, and S. Nasri (2001), The HYDROMED model and its application to semi-arid Mediterranean catchments with hill reservoirs: 2. Rainfall-runoff model applications to three Mediterranean hill reservoirs, *Hydrol. Earth Syst. Sci.*, *5*(4), 554–562.

Ramirez-Sanz, L., M. A. Casado, J. M. de Miguel, I. Castro, M. Costa, and F. D. Pineda (2000), Floristic relationship between scrubland and grassland patches in the Mediterranean landscape of the Iberian Peninsula, *Plant Ecol.*, *149*(1), 63–70.

Reichle, R. H., R. D. Koster, J. R. Dong, and A. A. Berg (2004), Global soil moisture from satellite observations, land surface models, and ground data: Implications for data assimilation, *J. Hydrometeorol.*, *5*(3), 430–442.

Reynolds, J., P. Kemp, and J. Tenhunen (2000), Effects of long-term rainfall variability on evapotranspiration and soil water distribution in the Chihuan desert: A modeling analysis, *Plant Ecol.*, *150*, 145–159.

Richards, J. A. (1999), *Remote Sensing Digital Image Analysis*, Springer, New York.

Rodriguez-Iturbe, I. (2000), Ecohydrology: A hydrologic perspective of climate-soil-vegetation dynamics, *Water Resour. Res.*, *36*(1), 3–9.

Sakcali, M. S., and M. Ozturk (2004), Eco-physiological behaviour of some mediterranean plants ad suitable candidates of degraded areas, *J. Arid Environ.*, *57*(2), 141–153.

Scanlon, T. M., J. D. Albertson, K. K. Caylor, and C. A. Williams (2002), Determining land surface fractional cover from NDVI and rainfall time series for a savanna ecosystem, *Remote Sens. Environ.*, *82*(2–3), 376–388.

Schmid, H. P. (1994), Source areas for scalars and scalar fluxes, *Boundary Layer Meteorol.*, *67*(3), 293–318.

Schmid, H. P. (1997), Experimental design for flux measurements: Matching scales of observations and fluxes, *Agric. For. Meteorol.*, *87*, 179–200.

Schmid, H. P. (2002), Footprint modelling for vegetation atmosphere exchange studies: A review and perspective, *Agric. For. Meteorol.*, *113*, 159–183.

Scholes, R. J., and S. R. Archer (1997), Tree-grass interactions in savannas, *Annu. Rev. Ecol. Syst.*, *28*, 517–544.

Shimabukuro, Y. E., V. C. Carvalho, and B. F. T. Rudorff (1997), NOAA-AVHRR data processing for the mapping of vegetation cover, *Int. J. Remote Sens.*, *18*(3), 671–677.

Sophocleous, M. (2000), From safe yield to sustainable development of water resources—The Kansas experience, *J. Hydrol.*, *235*(1–2), 27–43.

Su, Y., P. S. Huang, C. F. Lin, and T. M. Tu (2004), Approach to maximize increased details and minimize color distortion for IKONOS and QuickBird image fusion, *Opt. Eng.*, *43*(12), 3029–3037.

Tognetti, R., A. Longobucco, F. Miglietta, and A. Raschi (1998), Transpiration and stomatal behaviour of *Quercus ilex* plants during the summer in a Mediterranean carbon dioxide spring, *Plant Cell Environ.*, *21*(6), 613–622.

Twine, T. E., W. P. Kustas, J. M. Norman, D. R. Cook, P. R. Houser, T. P. Meyers, J. H. Prueger, P. J. Starks, and M. L. Wesely (2000), Correcting eddy-covariance flux underestimates over a grassland, *Agric. For. Meteorol.*, *103*(3), 279–300.

van Genuchten, M. T. (1980), A closed-form equation for predicting the hydraulic conductivity of unsaturated soils, *Soil Sci. Soc. Am. J.*, *44*(5), 892–898.

Ventura, F., P. R. Pisa, and E. Ardizzoni (2002), Temperature and precipitation trends in Bologna (Italy) from 1952 to 1999, *Atmos. Res.*, *61*(3), 203–214.

Verhoef, A., H. A. R. DeBruin, and B. VandenHurk (1997), Some practical notes on the parameter kB(−1) for sparse vegetation, *J. Appl. Meteorol.*, *36*(5), 560–572.

Vermote, E. F., D. Tanre, J. L. Deuze, M. Herman, and J. J. Morcrette (1997), Second simulation of the satellite signal in the solar spectrum, 6S: An overview, *IEEE Trans. Geosci. Remote*, *35*(3), 675–686.

Vesala, T., U. Rannik, M. Leclerc, T. Foken, and K. Sabelfeld (2004), Flux and concentration footprints, *Agric. For. Meteorol.*, *127*(3–4), 111–116.

Webb, E. K., G. I. Pearman, and R. Leuning (1980), Correction of flux measurements for density effects due to heat and water-vapor transfer, *Q. J. R. Meteorol. Soc.*, *106*(447), 85–100.

Western, A. W., R. B. Grayson, and G. Blöschl (2002), Scaling of soil moisture: A hydrologic perspective, *Annu. Rev. Earth Planet. Sci.*, *30*, 149–180.

Williams, C. A., and J. D. Albertson (2004), Soil moisture controls on canopy-scale water and carbon fluxes in an African savanna, *Water Resour. Res.*, *40*, W09302, doi:10.1029/2004WR003208.

J. D. Albertson and G. Katul, Department of Civil and Environmental Engineering, Pratt School of Engineering, Duke University, Durham, NC 27708, USA.

M. Detto, M. Mancini, and N. Montaldo, DIIAR, Fantoli Laboratory Building, Politecnico di Milano, Piazza Leonardo da Vinci, 32, I-20133 Milano, Italy. (nicola.montaldo@polimi.it)